INTERNATIONAL JOURNAL OF PRECISION ENGINEERING AND MANUFACTURING Vol. 17, No. 3, pp. 281-292 MARCH 2016 / 281
DOI: 10.1007/s12541-016-0036-6 ISSN 2234-7593 (Print) / ISSN 2005-4602 (Online)

The Modeling Approach of Digital Real Tooth Surfaces of Hypoid Gears based on Non-Geometric-Feature Segmentation and Interpolation Algorithm

Gang Li[1,#], Zhonghou Wang[1], and Aizoh Kubo[2]

1 School of Mechanical Engineering, University of Shanghai for Science and Technology, No. 516, Jungong Road, Yangpu, Shanghai, 200093, China
2 Research Institute for Applied Sciences, No. 49, Ooicho, Tanaka, Sakyouku, Kyoto, 606-8202, Japan
Corresponding Author / E-mail: ligangteller@163.com, TEL: +86-021-55277584, FAX: +86-021-55277584

KEYWORDS: Hypoid gears, Interpolation algorithms, Segmentation based on non-geometric-feature algorithm, Wear

A method for reconstructing the digital real tooth surfaces of hypoid gears can be a significant foundation for a variety of dynamic performance and lifetime prediction. This study demonstrates a new digital real tooth surfaces modeling approach for hypoid gears based on non-geometric-feature segmentation and interpolation algorithm. In this method, the discrete data points, which are obtained by using acoordinate measure machine (CMM), are segmented in the form of Delaunay triangular meshes. In order to identify irregular local micro-geometry features, the segmentation method starts with a feature detection based on normal vectors of Delaunay triangular meshes, identifying wear regions around each discrete data point, and is followed by region growing steps to divide tooth surface. In addition, a revised interpolation algorithm is applied to describe local micro-geometry features on wear regions via weighted factors to locally qualify the triangular vertexes. And the revised fairing algorithm minimizes the effect of noisy points. Experimental results from reconstruction of real tooth surface after wear test demonstrate that our method can improve the computation precision of wear region on actual tooth surfaces.

Manuscript received: June 22, 2015 / Revised: November 18, 2015 / Accepted: November 19, 2015

NOMENCLATURE

B = the recursion formula of basis function
E = pinion position error along the shaft offset direction
ΔE_m = blank offset
ΔE_i = deviation between the control vertex and interpolation curve
Δe = absolute error of position vector norm
G = axial displacement of the gear
J_i = moment of inertia
M_{ji}, L_{ji} = matrix of coordinate transformation from system $S_i$to system S_j
n = number of contact lines
N_g = number of the gear teeth
$n_{i,j}$ = normal vector of $V_{i,j}$
n_p, n_g = unit normal vectors in system S_t to profile of pinion and gear, respectively
$P(u_i)$ = interpolation curve
q= cradle rotation angle
R_a = ratio of roll
R_d = contact ratio of reference tooth surface
ΔR_p, ΔR_g = deviations between the actual tooth surface and the reference tooth surface
r_B = cutter radius
r_G = cutter point radius
r_p, r_g = position vectors in system S_t to profile of pinion and gear, respectively
S_a, S_b = coordinate systems for assisting the installment of the work piecen
S_c = machine cradle coordinate system
S_i = theareaof $Tri(i)$
S_m = cutting machine frame coordinate system
S_p, S_g = coordinate systems are attached to the pinion and the gear, respectively
S_t = the gear head-cutter coordinate system

s_r = radial setting
$Tri(i)$ = Delaunay triangle
t = time
t_i = position vector of control vertex
u = profile direction
u_p, u_g = surface parameters of the head-cutter to the pinion and the gear, respectively
V_{ij} = control points
v = tooth trace direction
v_{gt} = relative velocity vector of head-cutter to the gear
v_p, v_g = velocity vector of the pinion and the gear, respectively
ΔX_B = sliding base
ΔX_D = machine center to back
α_g = blade angle of the head-cutter
γ_m = machine root angle
κ = curve curvature
$l_i(j)$ = measure points
θ_p, θ_g = surface parameters of the head-cutter
δ_i = angle between normal vectors of Delaunay triangles
Γ_i = tangential vector
ω_i = weighted factor for control point
ω_p, ω_g = angular velocity of the pinion and the gear, respectively
ω_c = angular velocity of the cradle
Σ_p, Σ_g = generating surface of pinion and gear, respectively
ψ_p, ψ_g = current rotation angles of the pinion and the gear, respectively
ψ_c = current rotation angle of the cradle

1. Introduction

Hypoid gears are widely applied in aerospace, automotive etc.[1] As any other type of gearing, hypoid gears exhibit several types of failure modes including tooth breakage, scoring, pitting and surface wear.[2] Gear surface wear is a complex phenomenon that takes place in a relatively long period of time. Since the ratio of rolling and sliding motions changes along an instantaneous contact as well as with the path of contact, a non-uniform material removal through wear is inevitable, changing the tooth surface profiles to cause increased contact pressures. Such pressure increases further accelerate wear at the local contact region.[3] Hence, with the accumulation of wear, dynamic performance of the gear pair also changes negatively. The tooth surface meshing performance directly affects the overall performance of the drive system.

Many works have been directed towards the geometry, design, tooth contact analysis and manufacture of spiral bevel and hypoid gears in recent decades.[4-7] In order to predict the wear behavior of a gear pair, Archard's wear model was used widely and quite successfully in the past.[8-13]

With the development of numerical control technology, the actual machine settings and cutter dimensions allow precise calculation of the theoretical tooth surfaces.[18-20] However, the actual gear tooth surfaces deviate geometrically from the theoretical tooth surfaces due to manufacturing errors and heat treatment distortions. Gears having such deviations exhibit wear tendencies that are not uniform. Therefore, it is desirable to propose a digital tooth surface reconstruction approach for calculating local micro-geometry features of the actual gear tooth surfaces.

Park and Kahraman proposed a FE-based model based on a surface curve fitting method to capture the deviations from the theoretical nominal surfaces.[2] While this method was effective and accurate for representing global deviations due to manufacturing errors and heat treatment distortions, it might be difficult to represent local deviations such as wear in a certain region on the tooth surfaces. Kolivand and Kahraman developed acontact model to handle both local and global deviations via changes to the theoretical ease-off surface.[13] The curve fitting method calculated features on tooth surfaces by adjusting weighted local shape coefficients. But the weighted local shape coefficients were sensitive to noisy points. The fitting curves reduced the ability to detect small details.

Kubo et al. proposed a method for a non-generated face-milled hypoid gear reconstruction that utilized tooth surface data obtained from the scanning measurement.[14] And Takeda et al. developed a reconstruction method for a generated face-hobbed hypoid gear to analyze dynamic performance using similar approach with Kubo.[15] Gosselin et al. conducted hypoid gear lapping simulations using a wear model that employed a five-point parabolic interpolation algorithm for computing the actual tooth surface topography.[16,17] To evaluate tooth surface errors, gears were measured by CMM. However, constructing fair curve segments of hypoid gear tooth surfaces using parabolic interpolation is difficult due to the oscillatory nature of polynomials.

Most of previous works about complex spiral shape modeling mainly concentrated on approximating spiral arcsby polynomials, such as Cornu spirals, generalized Cornu spirals and logarithmic spirals.[21-25] Piegl proposed a method to determine the parameters by using Coons surface for the discrete data points.[22] However, the parameters determined by constructed Coons surface with unknown fitting surface deflection were not accurate. A method of constructing an approximation to a generalised Cornu spiral (GCS) arc using non-rational quintic Bézier curves matching end points, end slopes and end curvatures was presented by Cripps.[23] Sitnik developed a data segmentation algorithm based on the region-growing method.[24] It used large seed regions and selective region growing based on parameters ofthe best fit primitive. This multi-pass process was aided by histogram analysis of calculated features. An orientation analysis of the Gaussian map to area-form clusters was applied to identify hyperbolic and elliptical regions by Liu.[25] A signed point-to-plane distance function was used to identify noisy points of convex and concave regions.

All these approaches constructed the approximation based on minimizing the positional error between points on the spiral and corresponding points on the polynomial approximation. It was effective for reconstructing spiral surface based on point clouds with a large quantity of measurement points. However, in practice, the number of measurement points on tooth surface is limited. Even tooth surface topography by using parabolic interpolation algorithm[16,17] can exhibit unsatisfactory local micro-geometry features of the actual gear tooth surfaces.

This work focuses on presenting a revised NURBS (Non-Uniform Rational B-Splines) tooth surface reconstruction approach based on non-geometric-feature segmentation and revised interpolation algorithm of hypoid gears. This approach segments 3D data in the form of Delaunay triangular meshes. In order to identify irregular local micro-geometry features, local wear regions are grouped into areas of similar normal vectors. A segmentation algorithm for discrete data points based on the region-growing method is developed. By combining of NURBS curves interpolation algorithm with Delaunay triangulation, the measurement points or triangular vertexes are qualified by the local weighted factors, which are calculated by revised local interpolation algorithm. Therefore, non-geometric-feature segmentation algorithm reduces the calculation quantityof the revised local interpolation algorithm, in the meantime, revised local interpolation algorithm improves the accuracy of the segmentation algorithm.

2. Real Tooth Surface Model of Hypoid Gears

The purpose of this research is to reconstruct a real tooth surface model of hypoid gears by measuring the tooth surface. To achieve this, in this study, it is desirable to use a reference surface with an ideal contact condition for the gear performance. The reference surface of the gear is defined as the surface derived from the envelope of the gear cutter and that of the mating pinion at the conjugate surface of the gear. Therefore, the gear set with tooth surfaces conjugate to each other has tooth contact on the full tooth surface and has no transmission error.

2.1 Theoretical reference tooth surfaces

A general mathematical model for the generation of tooth surfaces of the gear is adopted as shown in Fig. 1.[26] Coordinate system S_g is rigidly attached to work piece (the gear). Coordinate system S_c is used to describe the angular position of the cradle. The coordinate system S_m is rigidly connected to the cutting machine frame. S_a and S_b are used for assisting the installment of the work piece. Coordinate system S_t is rigidly connected to the gear head-cutter. ψ_g and ψ_c are represent and related to the current rotation angles of the gear and the cradle, respectively.

There are six potential auxiliary motions parameters that can be used to modify the tooth surface of a generated spiral bevel gear: ΔE_m is blank offset, ΔX_B is sliding base, ΔX_D is machine center to back, γ_m is machine root angle, s_r is radial setting, and q is cradle rotation angle. The ratio of gear roll R_a is represented by the equation.

$$R_a = \frac{\omega_g}{\omega_c} = \frac{d\psi_g}{dt} \Big/ \frac{d\psi_c}{dt} \tag{1}$$

Where, ω_g and ω_c represent angular velocity of the gear and the cradle, respectively.

As shown in Fig. 2, the cutting edge of head-cutter blade is divided into four sections as the edge, toprem, profile, flankrem. The cutting surfaces of the head-cutter are generated by rotation of the blade about the Z_t-axis, the rotation angle is θ_g. Most of the generating of gear tooth surface is done by the profile section that is a straight line with the profile angle α_g. The fillet of the gear tooth surface is generated by the edge section with corner radius ρ_w. Referring to Fig. 2, an arbitrary

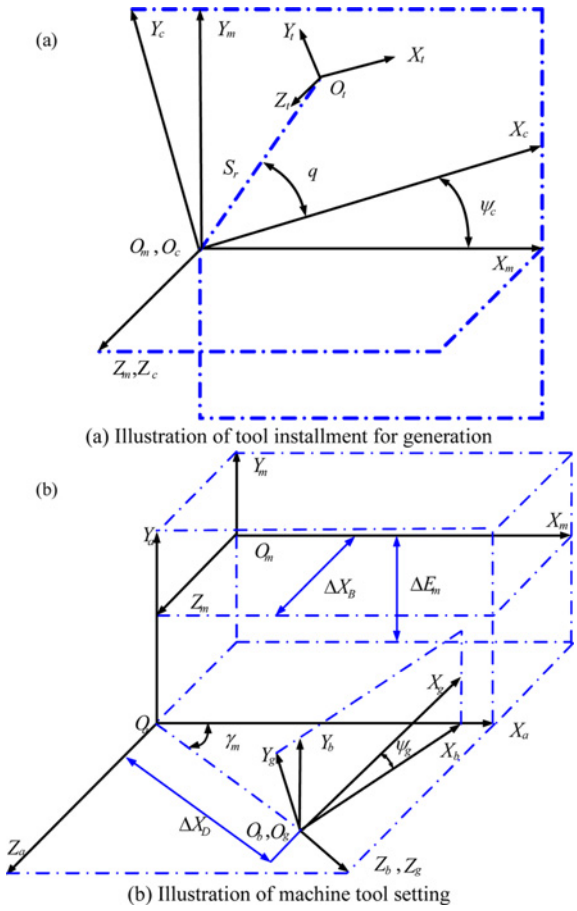

Fig. 1 Coordinate systems applied for gear generation

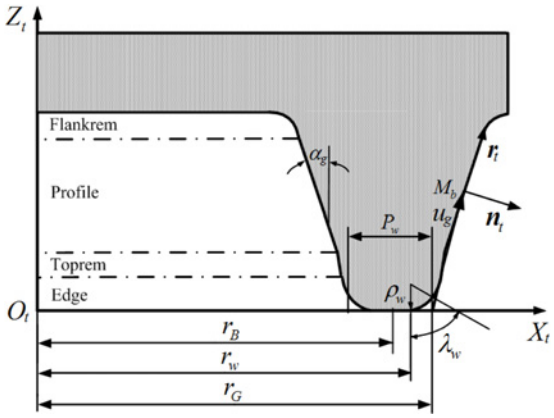

Fig. 2 The four sections of blades

point M_b on the cutting surface of blade is determined by u_g and $_g$ (Fig. 3). The generating surface Σ_g about the profile section of the head-cutter blade is represented by vector function $\boldsymbol{r}_t(u_g, \theta_g)$ as

$$r_t(u_g, \theta_g) = \begin{bmatrix} (r_G \pm u_g sin\alpha_g) cos\theta_g \\ (r_G \pm u_g sin\alpha_g) sin\theta_g \\ -u_g cos\alpha_g \end{bmatrix} \tag{2}$$

Where, r_G is the head-cutter point radius. α_g is the blade angle. u_g and θ_g are tooth surface parameters. The upper signs in Eq. (2) correspond

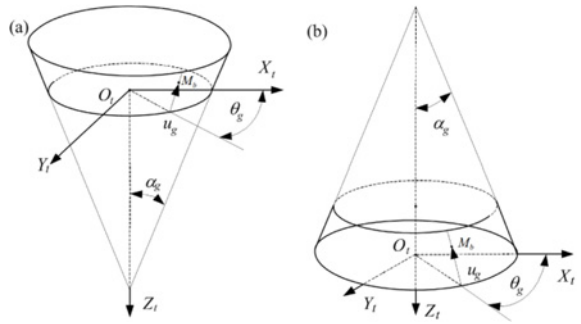

Fig. 3 Blades and generating cones for gear generating tool: (a) Generating tool cones for concave side and (b) Generating tool cones for convex side

to generation of concave side of the gear tooth surface, while the lower signs correspond to convex side.

The unit normal to the gear generating surface Σ_g is represented by vector function $\boldsymbol{n}_t(\theta_g)$ as

$$n_t(\theta_g) = \begin{bmatrix} cos\alpha_g cos\theta_g \\ cos\alpha_g sin\theta_g \\ \pm sin\alpha_g \end{bmatrix} \tag{3}$$

Gear theoretical tooth surface Σ_g is formed by cutting edge track surface Σ_t enveloping of cutter, so the theoretical tooth surface model can be represented as

$$\begin{cases} r_g(u_g, \theta_g, \psi_g) = M_{gt}(\psi_g) r_t(u_g, \theta_g) \\ n_g(u_g, \theta_g, \psi_g) = L_{gt}(\psi_g) n_t(u_g, \theta_g) \end{cases} \tag{4}$$

Where, M_{gt}, L_{gt} represent the transformation matrixes from coordinate S_t to S_g. ψ_g is rotation angle of the gear.

$$n_g \cdot v_{gt} = f_g(u_g, \theta_g, \psi_g) = 0 \tag{5}$$

Where, $\boldsymbol{v}_{gt}$ is the relative velocity vector of head-cutter to the gear.

The reference tooth surface of pinion which is the conjugate tooth surface of the gear theoretical reference tooth surface can be obtained by using the conjugate surface theory and meshing principle.[26]

2.2 Numerical analysis for digital real tooth surfaces

For reconstruction of real tooth surfaces, it is required to divide the reference surfaces to describe the reference tooth surfaces using grid points. As described in the previous section, a point on the cutting edge is taken, and the line generated by the point is calculated. All the lines generated by the points on the cutting edge are parallel to the root line, then the reference surface can be divided in the profile and lengthwise directions. The grid points of the tooth surface for a non-generated face-milled hypoid gear can be described by the points on the cutting edge and the rotational phase angles. And this approach was reported by Kubo et al..[14] However, the shapes of the paths of the points on the cutting edge are not straight lines but are curves in the generated face-hobbed progress. It becomes complicated and impractical to describe the reference surface of a generated face-hobbed hypoid gear using a point on the cutting edge and the cutter rotation angle.[15] For this reason, in this study, a method for describing the tooth surface using the theoretical contact lines is proposed,and this method is suitable to describe both the generated and non-generated hypoid gear using the grid points.

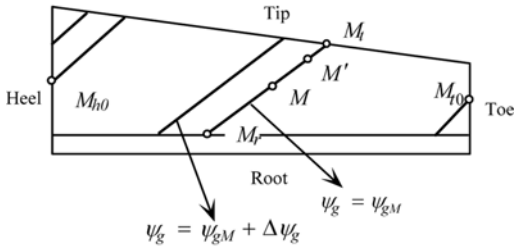

Fig. 4 Contact lines on reference tooth surface

As shown in Fig. 4, the point $M(u_{gM}, \theta_{gM})$ is the center of the gear tooth surface. The point $M_t(u_{gt}, \theta_{gt})$ is the intersection between the contact line through the point M and tip line.The distance from M_t to tip line can be represented as

$$f(u_{gt}, \theta_{gt}) = 0 \tag{6}$$

The current rotation angle of the gear $_{gt}$ can be represented as

$$g(u_{gt}, \theta_{gt}) = \psi_{gt}(u_{gt}, \theta_{gt}) - \psi_{gM} = 0 \tag{7}$$

Where, ψ_{gM} is the rotation angle of the gear corresponding to M_t.

With Eqs. (6)~(7), the coordinate of $M_t(u_{gt}, \theta_{gt})$ can be solved by Newton-Raphson Method.

Consider the distance from $M_t(u_{gi}, \theta_{gi})$ to tip line is $f(u_{gi}, \theta_{gi})$, and the current rotation angle ψ_{gi} is $g(u_{gi}, \theta_{gi})$.

We generate the M_{i+1} recursively by choosing step size Δu, $\Delta\theta$ and incrementing u_{gi}, θ_{gi} at each stage by Δu, $\Delta\theta$ respectively. So the equation satisfying $M_{i+1}(u_{gi}+\Delta u, \theta_{gi}+\Delta\theta)$ is given by

$$\begin{cases} 0 = f(u_{gi}+\Delta u, \theta_{gi}+\Delta\theta) = f(u_{gi}, \theta_{gi}) + \Delta u\left(\dfrac{\partial f}{\partial u_g}_i\right) + \Delta\theta\left(\dfrac{\partial f}{\partial \theta_g}_i\right) + \cdots \\ 0 = g(u_{gi}+\Delta u, \theta_{gi}+\Delta\theta) = g(u_{gi}, \theta_{gi}) + \Delta u\left(\dfrac{\partial g}{\partial u_g}_i\right) + \Delta\theta\left(\dfrac{\partial g}{\partial \theta_g}_i\right) + \cdots \end{cases} \tag{8}$$

as required.

Hence we have

$$\begin{cases} \left(\dfrac{\partial f}{\partial u_g}_i\right)\Delta u + \left(\dfrac{\partial f}{\partial \theta_g}_i\right)\Delta\theta = -f(u_{gi}, \theta_{gi}) \\ \left(\dfrac{\partial g}{\partial u_g}_i\right)\Delta u + \left(\dfrac{\partial g}{\partial \theta_g}_i\right)\Delta\theta = -g(u_{gi}, \theta_{gi}) \end{cases} \tag{9}$$

Then

$$\begin{cases} \Delta u = -\dfrac{-f(u_{gi}, \theta_{gi})\left(\dfrac{\partial g}{\partial \theta_g}_i\right) + g(u_{gi}, \theta_{gi})\left(\dfrac{\partial f}{\partial \theta_g}_i\right)}{\left(\dfrac{\partial f}{\partial u_g}_i\right)\left(\dfrac{\partial g}{\partial \theta_g}_i\right) - \left(\dfrac{\partial f}{\partial \theta_g}_i\right)\left(\dfrac{\partial g}{\partial u_g}_i\right)} \\ \Delta\theta = -\dfrac{-f(u_{gi}, \theta_{gi})\left(\dfrac{\partial g}{\partial u_g}_i\right) + g(u_{gi}, \theta_{gi})\left(\dfrac{\partial f}{\partial u_g}_i\right)}{\left(\dfrac{\partial f}{\partial u_g}_i\right)\left(\dfrac{\partial g}{\partial \theta_g}_i\right) - \left(\dfrac{\partial f}{\partial \theta_g}_i\right)\left(\dfrac{\partial g}{\partial u_g}_i\right)} \end{cases} \tag{10}$$

Here, the differential equations $\left(\dfrac{\partial f}{\partial u_g}_{i+1}\right)\left(\dfrac{\partial g}{\partial u_g}_{i+1}\right)\left(\dfrac{\partial f}{\partial \theta_g}_{i+1}\right)\left(\dfrac{\partial g}{\partial \theta_g}_{i+1}\right)$ can be represented as

$$\left(\frac{\partial f}{\partial u_g}\right)_{i+1} = \frac{f(u_{gi}+\Delta u, \theta_{gi}) - f(u_{gi}, \theta_{gi})}{\Delta u} \tag{11}$$

$$\left(\frac{\partial g}{\partial u_g}\right)_{i+1} = \frac{g(u_{gi}+\Delta u, \theta_{gi}) - g(u_{gi}, \theta_{gi})}{\Delta u} \tag{12}$$

$$\left(\frac{\partial f}{\partial \theta_g}\right)_{i+1} = \frac{f(u_{gi}, \theta_{gi}+\Delta\theta) - f(u_{gi}, \theta_{gi})}{\Delta\theta} \tag{13}$$

$$\left(\frac{\partial g}{\partial \theta_g}\right)_{i+1} = \frac{g(u_{gi}, \theta_{gi}+\Delta\theta) - g(u_{gi}, \theta_{gi})}{\Delta\theta} \tag{14}$$

Choosing Δu, $\Delta\theta$ small will improve the accuracy of the method, but it will be more time consuming excessively. Therefore, to reduce computation time, we need to determine the convergence precision on the algorithm. So, in this study, the convergenceprecisions are defined as

$$\left|f(u_{gi}, \theta_{gi})\right| \le 0.0001 \tag{15}$$

$$\left|\psi_g(u_{gi}, \theta_{gi}) - \psi_M\right| \le 0.0001 \tag{16}$$

The intersection M_r between contact line through the point M and root line also can be solved by the method mentioned above. With turning rotation angle of the gear ψ_g at regular intervals, in turn, the two endpoints of the corresponding contact line on conjugate reference tooth surface can be obtained.In this study, the distance between each contact line is equivalent to 1/16 of a pitch of the gear. The numerical analysis results of contact lines on reference tooth surfaces are shown in Fig. 5.

The contact ratio of driven side can be represented as

$$R_d = \frac{\left|\psi_{gt0} - \psi_{gh0}\right|}{\frac{2\pi}{N_g}} \tag{17}$$

Where, ψ_{gt0} is the rotation angle of M_{t0} in a meshing period. ψ_{gh0} is the rotation angle of M_{h0} in a meshing period. N_g is the number of the gear teeth.

Scanning lines are defined as l_i, i = 1, 2, …, n. Simultaneously, each contact line should be segmented and numbered from root to tip insequence, $l_i(j)$ j = 1, …, m, as shown in Fig. 6.

For describing deviationsof real tooth surfaces, it is required to measure the actual tooth surface by CMM. Unlike the measurement performed by scanning the line in both the profile direction and the tooth trace direction on the tooth surface, the measuring lines are set in contact lines direction, as shown in Fig. 6.

Given the possibility to numerical analysis of the results from 3D measurement with data obtained by CMM, we may define the gear and pinion coordinate systems, as shown in Fig. 7. The coordinates and unit normal vector of measurement point on the gear surface are (x_g, y_g, z_g) and ($\boldsymbol{n}_{xg}$, $\boldsymbol{n}_{yg}$, $\boldsymbol{n}_{zg}$), respectively. The coordinates and unit normal vector of measurement point on the pinion surface are (x_p, y_p, z_p) and ($\boldsymbol{n}_{xp}$, $\boldsymbol{n}_{yp}$, $\boldsymbol{n}_{zp}$), respectively.

The deviations between the actual tooth surface and the reference tooth surface can be represented as

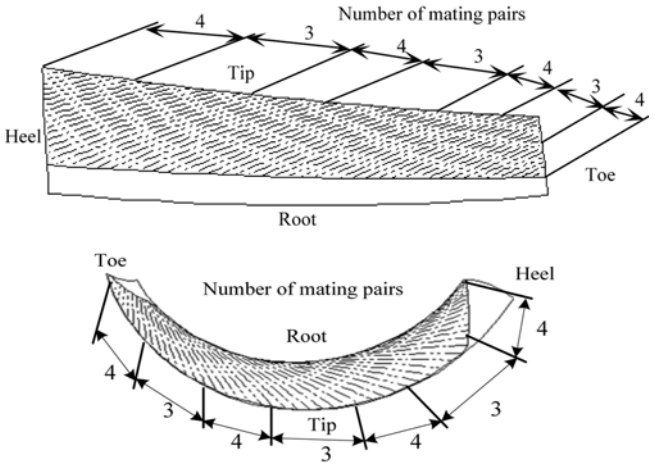

Fig. 5 Contact lines on the reference tooth surfaces (driving surface)

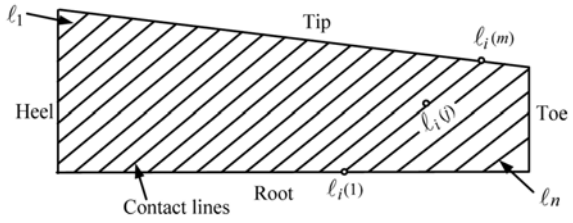

Fig. 6 Grid points on contact lines

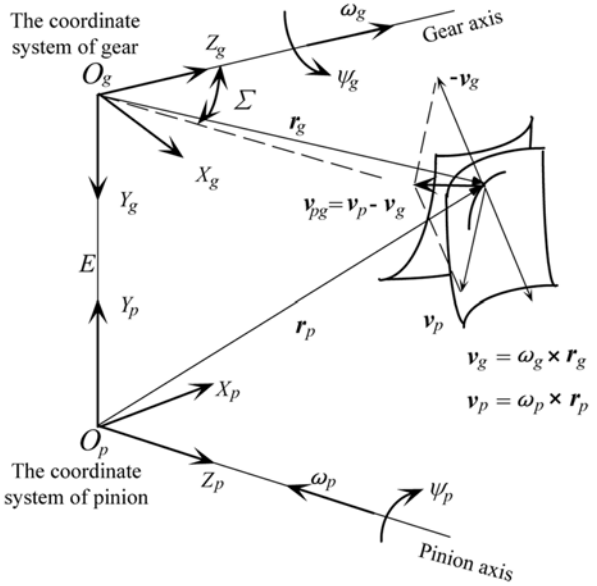

Fig. 7 Definition the gear and pinion coordinate systems

$$\Delta R_g = \Delta\theta_g \cdot (-y_g \cdot n_{xg} + x_g \cdot n_{yg}) \tag{18}$$

$$\Delta R_p = \Delta\theta_p \cdot (-y_p \cdot n_{xp} + x_p \cdot n_{yp}) \tag{19}$$

Where, $\Delta\theta_g$ and $\Delta\theta_p$ denote the angular deviations of the gear and

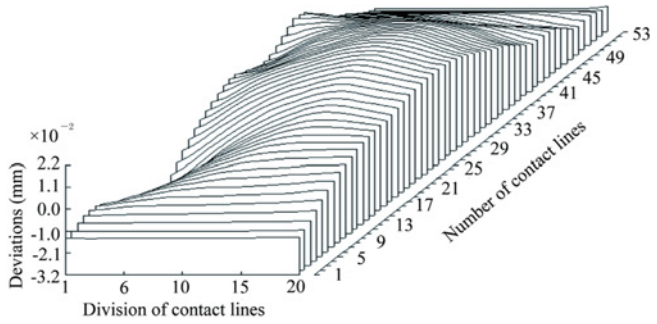

Fig. 8 Digital real tooth surface

the pinion, respectively. The real tooth surface model is shown in Fig. 8.

3. Real Tooth Surface Reconstruction Technology based on Non-Geometric-Feature Segmentation Algorithm

NURBS curves are a popular parametric form used in a variety of CAD/CAGD systems.[27] While in the current reconstruction process of real tooth surface, constructing fair curve segments using parametric polynomials is difficult due to alimiton the number of measurement points. Even NURBS curves can exhibit unsatisfactory curvature profiles. A different method of constructing a digital real tooth surface using non-geometric-feature segmentation of tooth surface discrete points is proposed. This method covers the real tooth surface with a collection of triangulation mesh in a consistent manner. To improve the interpolation algorithm speed of the real tooth surface, non-geometric-feature segmentation is used to split the discrete points along the growing path of triangulation or tooth surface edges.

In the process of computation of NURBS tooth surface, segmentation of discrete data points on tooth surface is necessary for describing geometric features of wear regions quickly and accurately. Traditional data segmentation divides the discrete data points into a set of defined surfaces, however, it is unsuitable for describing the irregular geometric features of wear regions. In this study, regions can be grouped into areas of similar normal vectors called center triangles. These center triangles are then grown to segment discrete data points.

3.1 Tooth surface model based on NURBS surface

NUBRS surface is based on the tensor product form of NURBS curve, the NURBS surface can be defined as[27]

$$P(u,v)=\frac{\sum_{i=1}^{m}\sum_{j=1}^{n}B_{i,k}(u)B_{j,k}(v)\omega_{ij}V_{ij}}{\sum_{i=1}^{m}\sum_{j=1}^{n}B_{i,k}(u)B_{j,k}(v)\omega_{ij}} \qquad (20)$$

$$u,v\in[0,1]$$

Where, $P(u, v)$ is the point on the surface for parametric values u and v. u, v denotes profile direction and the tooth trace direction, respectively. The grid of $(n+1)\times(m+1)$ control points is denoted by V_{ij}. The basis functions in u and v directions are denoted by $B_{i,k}$ and $B_{j,k}$. The variable k denotes the order of the surface in the direction of u and v. m and n are the numbers of control vertices in the direction of u and v, respectively.

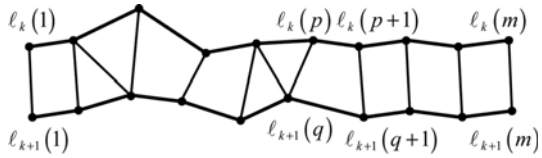

Fig. 9 Rough delaunay triangulation between adjacent scanning lines on tooth surface

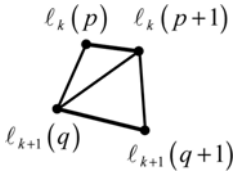

Fig. 10 The triangulates of polygon area

Wherein, the recursion formula of basis function can be defined as

$$\begin{cases} B_{i,0}(u)=\begin{cases}1, u_i\le u\le u_{i+1}\\ 0\end{cases} \\ B_{i,k}(u)=\dfrac{u-u_i}{u_{i+k}-u_i}B_{i,k-1}(u)+\dfrac{u_{i+k+1}-u}{u_{i+k+1}-u_{i+1}}B_{i+1,k-1}(u) \quad k\ge 1 \\ \dfrac{0}{0}=0 \end{cases} \qquad (21)$$

3.2 Delaunay triangulation for discrete data

In order to describe the real tooth surface intuitively, discrete data points obtainedby CMM are processed by using Delaunay triangulation principle.[28]

Traditional Delaunay triangulation algorithms tend to project geometric features in 3D discrete data points onto a 2D plane. Whereas triangular region obtained by this method cannot describe their spatial relations, the quality of triangulation is reduced. Therefore, this study presents direct triangulation algorithm on 3D discrete data points.

Scanning lines are defined as l_i, $i = 1, 2, \ldots, n$, the number of measure points on scanning lines is t, among which, two adjacent scanning lines are l_k, l_{k+1}, $1 \le k < k+1 \le n$. The number of measure points on two scanning lines is $l_k(j)$, $j = 1, 2, \ldots, m$, $l = l_{k+1}(l)$, $l = 1, 2, \ldots, m$.

As shown in Fig. 9, we connect the start points ($l_k(1)$ and $l_{k+1}(1)$), end points ($l_k(m)$ and $l_{k+1}(m)$) that belong to two scanning lines, respectively. And then, we connect each data point to neighborhood point which is the nearest on another scanning line in sequence. Simultaneously, the region between scanning lines l_k and l_{k+1} is divided into $r(r \ge t-1)$ spatialregions. This process may lead to the creation of regions which are quadrilateral.Therefore,the number of points in each region is checked.

For spatial quadrilateral regions, we triangulate them by the minimum interior angle maximum criterion[28] to complete the Delaunay triangulation of discrete data points on tooth surface, as shown in Fig. 10.

3.3 The normal vector of arbitrary point on tooth surface

During the gear measurement, the data measured by measurement

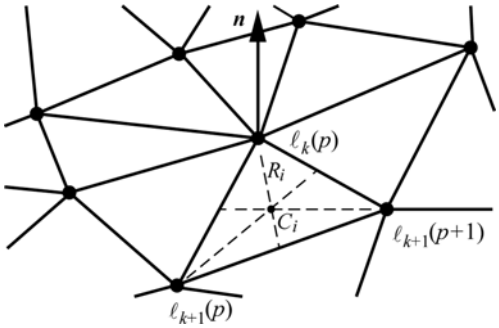

Fig. 11 The moment of inertia method to solve the normal vector

instrument is the coordinates of measure probe center.In order to obtain normal vector of an arbitrary point on tooth surface accurately, all neighborhood triangles with a common vertex $l_k(p)$ are defined as $Tri(i)$. The neighborhood triangle $Tri(i)$ as a spatial triangle mesh of approximating surface represents geometric feature changes of adjacent region around vertex $l_k(p)$.

Suppose material of adjacent regions around vertex $l_k(p)$ is homogeneous. The moment of inertia of $Tri(i)$ rotation about axis which is through the vertex $l_k(p)$ is defined as $\boldsymbol{J}_i$. The normal vector of vertex $l_k(p)$ is defined as $\boldsymbol{n}$. The center of gravity of neighborhood triangle $Tri(i)$ is defined as C_i. The moment of inertia for $Tri(i)$ rotation about $\boldsymbol{n}$ is represented as

$$J_i = S_i R_i^2 \tag{22}$$

Where, S_i is theareaof $Tri(i)$. R_i is the distance from the center of gravity C_i to $\boldsymbol{n}$.

The moment of inertia for all neighborhood triangles rotation about $\boldsymbol{n}$ is represented as

$$J = \sum_{i=1}^{n} S_i R_i^2 \tag{23}$$

Accordingto multi-rigid-body dynamics, the moment of inertia $\boldsymbol{J}$ can obtain extremum on three mutually perpendicular principal axes of inertia. The direction of the principal axis of inertia on which the moment of inertia $\boldsymbol{J}$ is the maximum among principal axes of inertia is the direction of the normal vector of vertex $l_k(p)$.

3.4 Region growing

Suppose an arbitrary triangle on digital real tooth surface as center triangle *CenTri*, normal vector of which is $\boldsymbol{n}$, the normal vector of whose adjacent triangles $NeiTri(i)$ are $\boldsymbol{n}_i i$ = 1,2,3. The angle between $\boldsymbol{n}$ and $\boldsymbol{n}_i$ is $_i$. Calculate the value T of each *CenTri* as Eq. (24). Compare all the T value bytraversing all *CenTri*s. One *CenTri* that the T value issmallest shall be defined as the *StaTri*, as shown in Fig. 12.

$$T = max(|\delta_1 - \delta_2|, |\delta_2 - \delta_3|, |\delta_1 - \delta_3|) - min(|\delta_1 - \delta_2|, |\delta_2 - \delta_3|, |\delta_1 - \delta_3|) \tag{24}$$

We calculate the normal vector of each adjacent triangle $NeiTri(i)$, and then, compare theangles betweenthenormal vectors of $NeiTri(i)$ and *CenTri*. The adjacent triangle $NeiTri(i)$, which normal vectorial angle is minimum among adjacent triangles, is defined as the next *CenTri*.

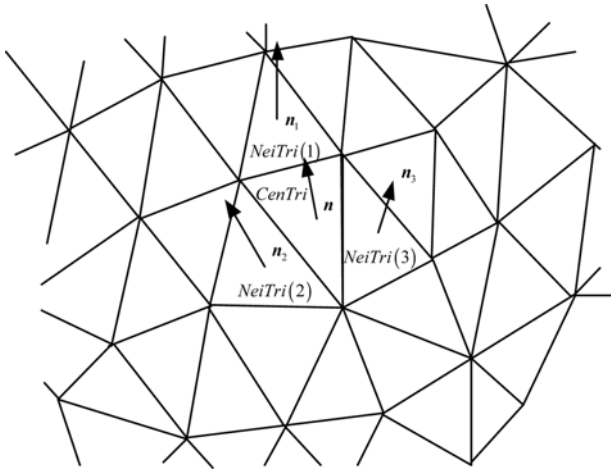

Fig. 12 The position of *CenTri* on tooth surface

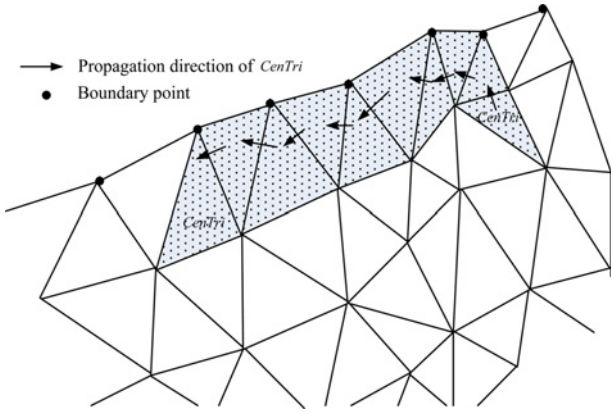

Fig. 13 The process of segmentation of discrete data based on non-geometric-feature

Otherwise, we reselect start triangle *StaTri*. (Fig. 13).

Region growing is performed until there are no more possible triangular regions that can be added. It can also be used to aid shape recognition for wear regions.

3.5 Revised local interpolation algorithm

The traditional NURBS surface interpolation algorithm is curve interpolating first, curvefairness second. Most of works calculated features of NURBS surfaces via local weighted factors to locally qualify control vertexes. It is difficult to guarantee precision of real tooth surface reconstruction with wear due to the oscillatory nature of polynomials caused by deviation of wear regions.

The local interpolation algorithm proposed in this study overcomes these limitations and in addition, provides a unified high-performance solution to the computation of NURBS surfaces by adjusting local weighted factors and deviation of control vertices, simultaneously.

According to the non-geometric-feature segmentation algorithm of discrete data points, grids which are not satisfied with Eq. (24) are extracted from tooth surface as object to interpolation.

The control vertex V_i of interpolation curve $P(u_i)$ is obtained by interpolation algorithm. The corresponding weighted factor is ω_i. ΔE_i is

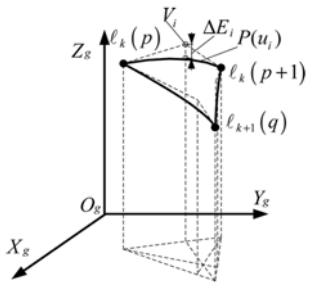

Fig. 14 Revised interpolation algorithm of tooth surface

the deviation between the control vertex V_i and interpolation curve $P(u_i)$, as shown in Fig. 14.

$$\begin{aligned}&\Sigma B_{i,k}(u_j)(\omega_i+\Delta\omega_i)\Delta V_i+\Sigma B_{i,k}(u_j)\Delta\omega_i(B_i-V_i)\\&=\Sigma B_{i,k}(u_j)\omega_i(V_i-V(u_j))\end{aligned} \tag{25}$$

Where, V_i is a control vertex. ΔV_i is the deviation of curve control vertex V_i. ω_i is the weighted factor for V_i. $\Delta\omega_i$ is the weighted factor deviation of ω_i. $B_{i,k}$ is the k order B-spline basis function in u direction.

For the compensation of ΔE_i on NURBS surface, it is necessary to adjust the positions of control vertices. Based on thrice interpolation algorithm of NURBS surface for position compensation of control vertices, the deviations of control vertices can be solved by ($\Delta\omega_i$=0)

$$\begin{pmatrix} b_{1,2}\,b_{1,3} & 0 & & & 0\\ b_{2,2}\,b_{2,3}\,b_{2,4} & & & & 0\\ & \cdots & & & \\ & b_{j,j+1}\,b_{j,j}\,b_{j,j+1} & & & \cdots\\ \cdots & & \cdots & & \\ & & & b_{n-1,n-1}\,b_{n-1,n}\,b_{n-1,n+1} & \\ 0 & & & b_{n,n} \quad b_{n,n+1} & \end{pmatrix} \tag{26}$$

$$\begin{pmatrix}\Delta V_2\\ \Delta V_3\\ \cdots\\ \Delta V_{n+1}\end{pmatrix}=\begin{pmatrix}a_1\Delta E_1\\ a_2\Delta E_2\\ \cdots\\ a_n\Delta E_n\end{pmatrix}$$

Where, $a_j=\Sigma B_{i,3}(u_j)\omega_i$. $b_{j,i}=\Sigma B_{i,3}(u_j)\omega_i$.

The deviations of weighted factors of control vertices can be solved by ($\Delta V_i=0$)

$$\begin{pmatrix} Q_{1,2}\,Q_{1,3} & 0 & & & 0\\ Q_{2,2}\,Q_{2,3}\,Q_{2,4} & & & & 0\\ & \cdots & & & \\ & Q_{j,j+1}\,Q_{j,j}\,Q_{j,j+1} & & & \cdots\\ \cdots & & \cdots & & \\ & & & Q_{n-1,n-1}\,Q_{n-1,n}\,Q_{n-1,n+1} & \\ 0 & & & Q_{n,n} \quad Q_{n,n+1} & \end{pmatrix} \tag{27}$$

$$\begin{pmatrix}\Delta\omega_2\\ \Delta\omega_3\\ \cdots\\ \Delta\omega_{n+1}\end{pmatrix}=\begin{pmatrix}\Sigma n_{i,3}(u_1)\omega_1\Delta E_1\\ \Sigma n_{i,3}(u_2)\omega_2\Delta E_2\\ \cdots\\ \Sigma n_{i,3}(u_n)\omega_n\Delta E_n\end{pmatrix}$$

Where, $Q_{j,i}=\Gamma_i\cdot B_{i,3}(u_j)\Delta E_i$. Γ_i is the tangential vector of V_i-$V(u_i)$. $\boldsymbol{n}_{i,3}$ is the normal vector of $V_{i,3}$.

4. Fairing Algorithm

To minimize the effect of noisy points, most of fairing algorithms for discrete data points use calculated curvature of interpolation curve to distinguish noisy points, then delete them. These methods are unable to guarantee modelingprecision of local geometric features of wear regions on the tooth surface.

The shape of the curve must be modified as interpolation points have changed. Surely local geometric features of wear regions can be determined automatically by control vertices, so the solution is to make sure which control vertices should be adjusted and how many minimal adjustments can guarantee fairness.

The curvature of corresponding interpolation curve $P(u_i)$ of control vertex V_i is defined as[27]

$$\kappa(u_i)=\frac{\left|\dot{P}(u_i)\times\ddot{P}(u_i)\right|}{\left|\dot{P}(u_i)\right|^3} \tag{28}$$

Where, $\dot{P}(u_i)$ is the first derivative of $P(u_i)$. $\ddot{P}(u_i)$ is the second derivative of $P(u_i)$.

The curvature of corresponding data point of each control vertex can be solved by using Eq. (28). The judging standard for noisy point is the curvature changes among data points. If the curvature of corresponding data point of control vertex V_i meets Eq. (29), then judge it as a noisy point.

$$\begin{cases}\Delta\kappa(u_{i-1})\cdot\Delta\kappa(u_i)<0\\ \Delta\kappa(u_i)\cdot\Delta\kappa(u_{i+1})<0\end{cases} \tag{29}$$

Here, $\Delta\kappa(u_i)=\kappa(u_i)-\kappa(u_{i-1})$.

Suppose the control vertex V_j as the judged noisy point, the corresponding position vector of V_j is $\boldsymbol{t}_j$. The new control vertex V_j' is defined as

$$V_j'=\frac{(t_{j+2}-t_j)l_j+(t_j-r_{j-2})h_j}{t_{j+2}-t_{j-2}} \tag{30}$$

Where, $l_j=\dfrac{(t_{j+1}-t_{j-3})V_{j-1}+(t_{j+1}-t_j)V_{j-2}}{t_j-t_{j-3}}$;

$h_j=\dfrac{(t_{j+3}-t_{j-1})V_{j+1}-(t_j-t_{j-1})V_{j+2}}{t_{j+3}-t_j}$

The fairingprocedure of discrete points on the tooth surface can be achieved by using Eq. (30). And it greatly improves the effect of real tooth surface construction via combines with local interpolation algorithm based on non-geometric-feature segmentation algorithm.

5. Experimental Work and Calculation Results

In order to verify the validity and accuracy of the above algorithm, several experiments were performed. The hypoid gear geometry parameters and machine-tool settings are shown in Table 1 and 2, respectively.

Hypoid gear box wear tests are done in loaded rear axle testing machine. The input speed of pinion is 4000 rmin, and the input torque is 160 N·m. In the test, in order to accelerate the tooth surface wear, and savethetest time, some grinding powder is added in the lubricating oil artificially. The results of tooth surface wear test are shown in Fig. 15.

Table 1 The geometric parameters of hypoid gears

Parameters	Pinion	Gear
Number of teeth	6	37
Module	8.243	
Hand of spiral	Left-hand	Right-hand
Shaft angle /(°)	90	
Pinion offset /mm	31.75	
Face width /mm	45.12	40
Pitch angle	11°43'	77°58'
Face angle	16°3'	78°26'
Root angle	11°15'	73°31'
Pitch apex beyond cross point /mm	0.71	1.40
Face apex beyond cross point/mm	-3.14	1.40
Root apex beyond cross point /mm	-7.59	1.39
Outer cone distance /mm	155.35	155.92
Outside diameter /mm	84.07	305.52
Pitch diameter /mm	304.99	

Table 2 The adjustment parameters of pinion machine-tool

Parameters	Concave side	Convex side
Cutter diameter /inch	8.94	8.73
Blade angle / (°)	14	35
Machine root angle	-3°	-4°5'
Machine center to back /mm	5.26	10.57
Sliding base /mm	22.60	37.56
Blank offset /mm	25.51	44.64
Eccentric angle	55°53'	68°4'
Swivel angle	269°33'	292°21'
Cutter spindle rotation angle	49°24'	54°56'
Ratio of roll	0.6802	0.8301

(In the test, 150 mg grinding powder is added in 1.3 L lubricating oil.)

The Hyb-35 hypoid gear tooth surface measuring instrument is used in this test for scanning measurement. The computation of tooth surface based on the interpolation algorithm proposed by literature[14,15] is shown in Fig. 16. The computation of tooth surface based on the presented method is shown in Fig. 17, and variables used for this method are listed in Table 3.

On the basis of data points on hypoid gear real tooth surface Σ_r, compare the digital model of gear tooth surface based on area weighting interpolation algorithm and proposed approach with data points on the surface tooth Σ_r, respectively. During the error analysis of digital gear tooth surface model, we focus on the calibration of measurement point data in tooth surface wear region. According to the results of tooth surface wear test, the determined data validation area is shown in Fig. 18.

The position vector norm of point p_i in calibration area on NURBS tooth surface based on non-geometric-feature segmentation is $r_i = \sqrt{x_i^2+y_i^2+z_i^2}$. The position vector norm of the corresponding point p_i' on actual tooth surface Σ_r is $r_{mi}^* = \sqrt{x'^2_i+y'^2_i+z'^2_i}$. The absolute error of position vector norm between point p_i in NURBS tooth surface and corresponding point p_i' on actual tooth surface is $\Delta e = \left| r_{mi}^* - r_i \right|$.

In this study, we choose 4 measure lines for verification precision of two digital real tooth surface computation methods, as shown in Fig. 18. The location diameters of Line1, Line 2, Line 3 and Line 4 are 305.30 mm, 305.10 mm, 304.90 mm and 304.70 mm, respectively. The absolute errors on that 4 measure lines after running 2000km and 5000 km are shown in Fig. 19 and 20, respectively. Some detailed results are

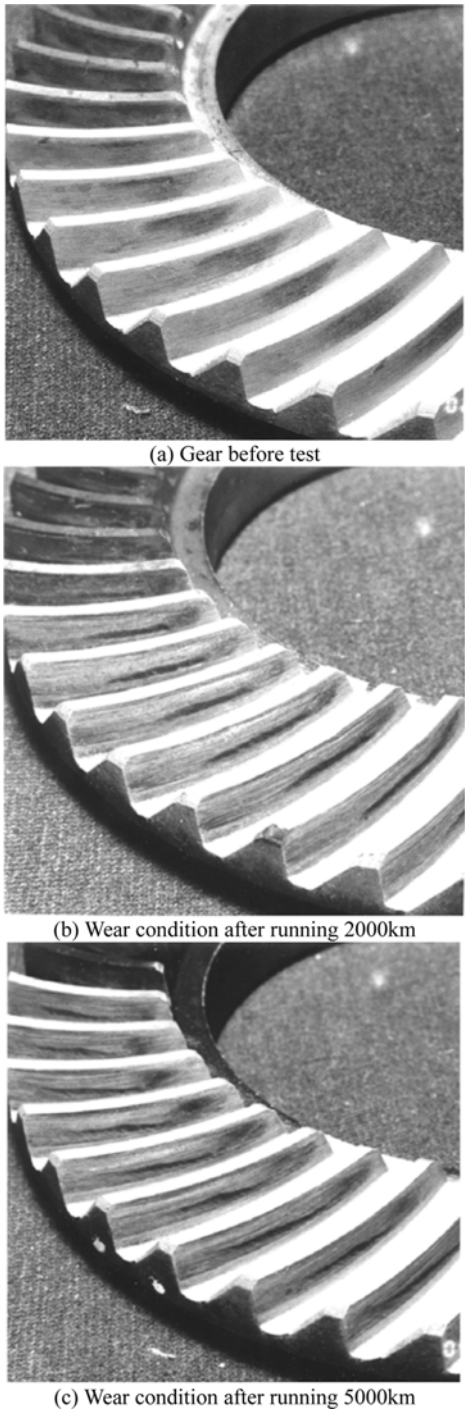

(a) Gear before test

(b) Wear condition after running 2000km

(c) Wear condition after running 5000km

Fig. 15 Wear condition of test gear tooth surface

Table 3 The parameters of method proposed in this study

Parameters	Computation object	
	2000 km	5000 km
rotation angle ψ_{gf0} / rad	3.143	
rotation angle ψ_{gh0} / rad	3.692	
contact ratio R_d	3.498	
Number of contact lines	53	
Number of measure lines	17	
Order of B-spline	3	
Weighted factor deviation $\Delta\omega_i$	≤0.064	≤0.083
Deviation of curve control vertex V_i / μm	≤0.79	≤1.04

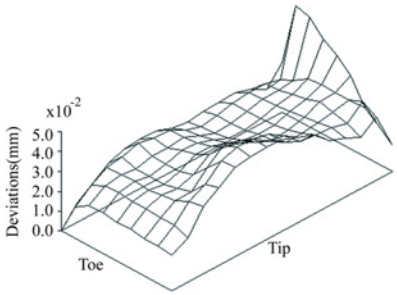

(a) Computation of wear tooth surface after running 2000km

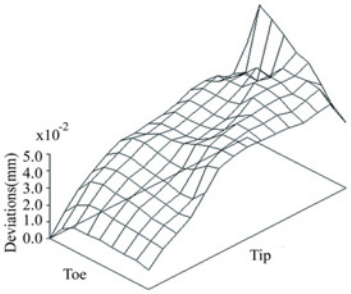

(b) Computation of wear tooth surface after running 5000km

Fig. 16 Computation tooth surface based on the area weighting interpolation algorithm (the gear)

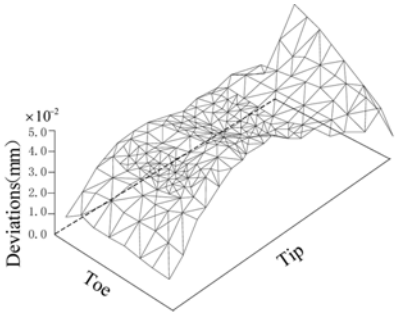

(a) Computation of wear tooth surface after running 2000km

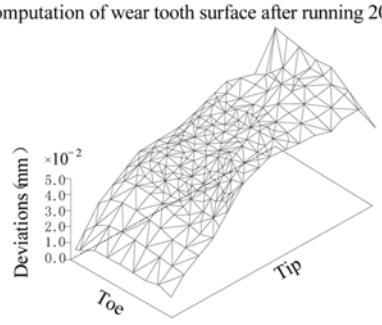

(b) Computation of wear tooth surface after running 5000km

Fig. 17 Computation tooth surface based on non-geometric-feature segmentation and interpolation algorithm (the gear)

listed in Table 4.

The average absolute errors of computation tooth surface based on the area weighting interpolation method are 2.18 m and 4.64 m after 2000 km and 5000 km wear test, respectively, while the absolute errors of this study are only 1.23 m and 2.42 m. After running 5000 km, the maximum absolute error on NURBS tooth surface computed by area weighting interpolation algorithm is 9.4 m, while the maximum absolute

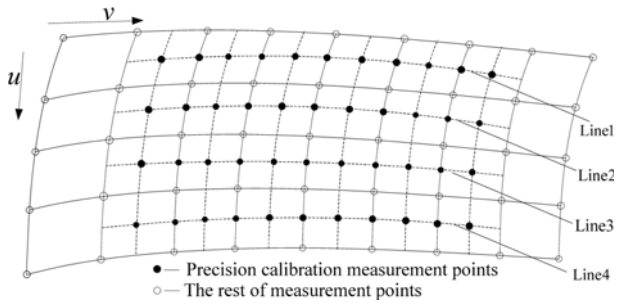

Fig. 18 Precision calibration measurement points on digital tooth surface

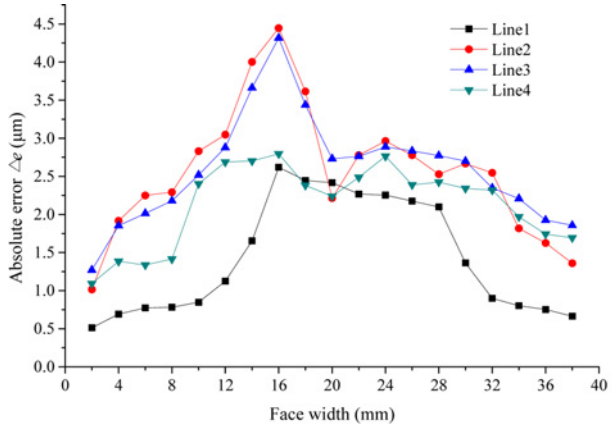

(a) The average errors of area weighting interpolation algorithm

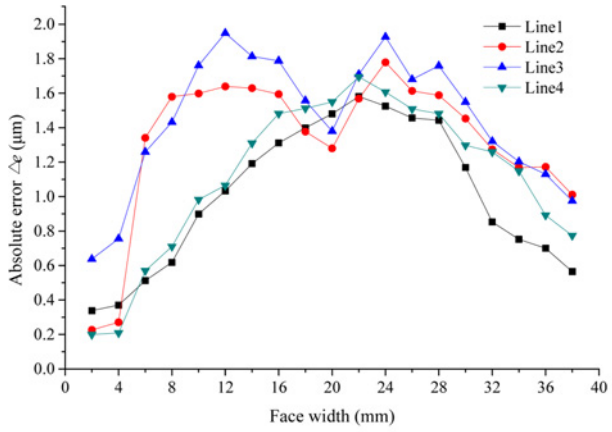

(b) The average errors of the method proposed in this study

Fig. 19 The average errors of computation after running 2000 km

error on NURBS tooth surface computed by non-geometric-feature segmentation and interpolation algorithm is less than 3.6 m. Therefore, it is obvious that the presented method improves the computation precision of wear region on actual tooth surfaces.

6. Conclusions

We propose a NURBS reconstruction approach for hypoid gear tooth surfaces that based on non-geometric-feature segmentation algorithm.

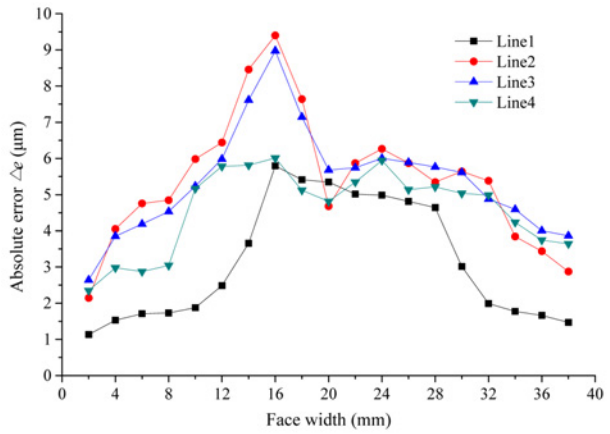

(a) The average errors of area weighting interpolation algorithm

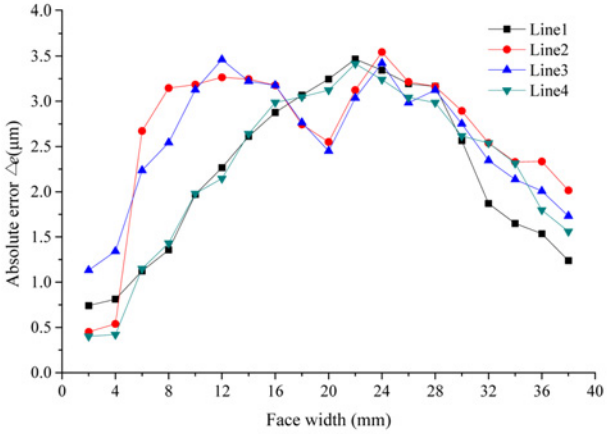

(b) The average errors of the method proposed in this study

Fig. 20 The average errors of computation after running 5000 km

Table 4 Comparison of our method against existing approach using area weighting interpolation algorithm

Parameters		Area weighting interpolation algorithm	Method proposed in this study
Number of points	2000 km	135	192
	5000 km	135	231
Number of meshes	2000 km	112	276
	5000 km	112	314
Calculation time / s	2000 km	3	5
	5000 km	3	8
Area ratio of local segmented regions	2000 km	0%	36.9%
	5000 km	0%	40.1%
Average absolute errors / μm	2000 km	2.18	1.23
	5000 km	4.64	2.42
Maximum absolute errors / μm	2000 km	4.32	1.95
	5000 km	9.40	3.57

Our approach isto create an algorithm that could process discrete data of wear regions obtained by CMM with equal ease. For this we adopt the region-growing algorithm based on Delaunay triangulationfor real tooth surface calculation. The segmentation algorithm can automatically identify wear regions of measured discrete data on tooth surfaces.

The segmentation algorithm has some characteristics as follows: First, the region-growing algorithm can recognize wear regions on tooth surfaces. Only the regions which are produced due to the rough effect in normal vectors are extracted in the local interpolation process. Hence, the algorithm can reduce time-consuming steps ininterpolation algorithm. Second, a revised local interpolation algorithm is applied to compute local deviations in wear regions on tooth surfaces. This local interpolation algorithm compensates for modeling error ΔE_i via control vertices and weighted factors rectification. That is more accurately to represent local micro-geometry features. Finally, NURBS fitting algorithm reduces sensitivity to noisy points.

The results of test show the applicability of this approach for real tooth surface reconstruction of hypoid gears. Future directions of work include optimizing threshold value in segmentation algorithm to minimize over-segmentation. We will also investigate techniques in interconnectivity relationships between wear prediction model and micro-geometry features based on this digital real tooth surfaces reconstruction approach.

ACKNOWLEDGEMENT

The authors acknowledge the financial support from the Natural Science Foundation of China (NSFC) for their financial support of the research under Contract No.51075279.

REFERENCES

1. Chen, B., Liang, D., and Li, Z., "A Study on Geometry Design of Spiral Bevel Gears based on Conjugate Curves," Int. J. Precis. Eng. Manuf., Vol. 15, No. 3, pp. 477-482, 2014.
2. Park, D. and Kahraman, A., "A Surface Wear Model for Hypoid Gear Pairs," Wear, Vol. 267, No. 9, pp. 1595-1604, 2009.
3. Park, D., Kolivand, M., and Kahraman, A., "An Approximate Method to Predict Surface Wear of Hypoid Gears using Surface Interpolation," Mechanism and Machine Theory, Vol. 71, pp. 64-78, 2014.
4. Zhang, Q., Kang, J., Dong, W., and Lyu, S., "A Study on Tooth Modification and Radiation Noise of a Manual Transaxle," Int. J. Precis. Eng. Manuf., Vol. 13, No. 6, pp. 1013-1020, 2012.
5. Litvin, F. L., Fuentes, A., Fan, Q., and Handschuh, R. F., "Computerized Design, Simulation of Meshing, and Contact and Stress Analysis of Face-Milled Formate Generated Spiral Bevel Gears," Mechanism and Machine Theory, Vol. 37, No. 5, pp. 441-459, 2002.
6. Tsai, Y.-C. and Hsu, W.-Y., "The Study on the Design of Spiral Bevel Gear Sets with Circular-Arc Contact Paths and Tooth Profiles," Mechanism and Machine Theory, Vol. 43, No. 9, pp. 1158-1174, 2008.
7. Litvin, F. L., Fuentes, A., and Hayasaka, K., "Design, Manufacture, Stress Analysis, and Experimental Tests of Low-Noise High Endurance Spiral Bevel Gears," Mechanism and Machine Theory,

Vol. 41, No. 1, pp. 83-118, 2006.

8. Flodin, A. and Andersson, S., "Simulation of Mild Wear in Helical Gears," Wear, Vol. 241, No. 2, pp. 123-128, 2000.
9. Flodin, A. and Andersson, S., "A Simplified Model for Wear Prediction in Helical Gears," Wear, Vol. 249, No. 3, pp. 285-292, 2001.
10. Bajpai, P., Kahraman, A., and Anderson, N., "A Surface Wear Prediction Methodology for Parallel-Axis Gear Pairs," Journal of Tribology, Vol. 126, No. 3, pp. 597-605, 2004.
11. Kahraman, A., Bajpai, P., and Anderson, N., "Influence of Tooth Profile Deviations on Helical Gear Wear," Journal of Mechanical Design, Vol. 127, No. 4, pp. 656-663, 2005.
12. Park, D., Kolivand, M., and Kahraman, A., "Prediction of Surface Wear of Hypoid Gears using a Semi-Analytical Contact Model," Mechanism and Machine Theory, Vol. 52, pp. 180-194, 2012.
13. Kolivand, M. and Kahraman, A., "An Ease-Off based Method for Loaded Tooth Contact Analysis of Hypoid Gears Having Local and Global Surface Deviations," Journal of Mechanical Design, Vol. 132, No. 7, Paper No. 071004, 2010.
14. Kubo, A., Tarutani, I., Gosselin, C., Nonaka, T., Aoyama, N., and Wang, Z., "On Simulation Methods of Performance of Hypoid and Spiral Bevel Gears," Transactions of the JSME, Series C, Vol. 62, No. 599, pp. 2833-2850, 1996.
15. Takeda, R., Komori, M., Nishino, T., Kimura, Y., Nishino, T., et al., "Performance Analysis of Generated Hypoid Gear based on Measured Tooth Flank Form Data," Mechanism and Machine Theory, Vol. 72, No. pp. 1-16, 2014.
16. Jiang, Q., Gosselin, C., and Masseth, J., "Simulation of Hypoid Gear Lapping," Journal of Mechanical Design, Vol. 130, No. 11, Paper No. 112601, 2008.
17. Jiang, Q., Gosselin, C., and Masseth, J., "Computer-Aided Machine Setting for Lapping Optimization," Journal of Mechanical Design, Vol. 131, No. 3, Paper No. 031003, 2009.
18. Abbas, A. T. M., "Enhanced CNC Machines Capabilities by Adding Circular Patterns Cycle," Int. J. Precis. Eng. Manuf., Vol. 13, No. 10, pp. 1753-1758, 2012.
19. Simon, V. V., "Influence of Tooth Modifications on Tooth Contact in Face-Hobbed Spiral Bevel Gears," Mechanism and Machine Theory, Vol. 46, No. 12, pp. 1980-1998, 2011.
20. Yun, J.-H., Jeong, M.-S., Lee, S.-K., Jeon, J.-W., Park, J.-Y., and Kim, G. M., "Sustainable Production of Helical Pinion Gears: Environmental Effects and Product Quality," Int. J. Precis. Eng. Manuf.-Green Tech., Vol. 1, No. 1, pp. 37-41, 2014.
21. Meek, D. S. and Walton, D. J., "An Arc Spline Approximation to a Clothoid," Journal of Computational and Applied Mathematics, Vol. 170, No. 1, pp. 59-77, 2004.
22. Piegl, L. A. and Tiller, W., "Parametrization for Surface Fitting in Reverse Engineering," Computer-Aided Design, Vol. 33, No. 8, pp. 593-603, 2001.
23. Cripps, R. J., Hussain, M. Z., and Zhu, S., "Smooth Polynomial Approximation of Spiral Arcs," Journal of Computational and Applied Mathematics, Vol. 233, No. 9, pp. 2227-2234, 2010.
24. Sitnik, R. and Błaszczyk, P. M., "Segmentation of Unsorted Cloud of Points Data from Full Field Optical Measurement for Metrological Validation," Computers in Industry, Vol. 63, No. 1, pp. 30-44, 2012.
25. Liu, Y. and Xiong, Y., "Automatic Segmentation of Unorganized Noisy Point Clouds based on the Gaussian Map," Computer-Aided Design, Vol. 40, No. 5, pp. 576-594, 2008.
26. Litvin, F. L. and Fuentes, A., "Gear Geometry and Applied Theory," Cambridge University Press, pp. 97-118, 2004.
27. Tang, K. and Pang, A., "Optimal Connection of Loops in Laminated Object Manufacturing," Computer-Aided Design, Vol. 35, No. 11, pp. 1011-1022, 2003.
28. Woo, H., Kang, E., Wang, S., and Lee, K. H., "A New Segmentation Method for Point Cloud Data," International Journal of Machine Tools and Manufacture, Vol. 42, No. 2, pp. 167-178, 2002.